Analysis of Viscoelastic Behavior and Dynamic Mechanical Relaxation of Copolyester Based Layered Silicate Nanocomposites using Havriliak–Negami Model

RAJENDRA A. KALGAONKAR, SOMNATH NANDI, SANJEEV S. TAMBE, JYOTI P. JOG*

Chemical Engineering Division, National Chemical Laboratory, Pune 411 008, India

Received 11 July 2003; revised 27 February 2004; accepted 4 March 2004
DOI: 10.1002/polb.20128
Published online in Wiley InterScience (www.interscience.wiley.com).

ABSTRACT: The solid-state viscoelastic properties are examined for intercalated nanocomposites based on a copolyester and (2-ethyl-hexyl)dimethyl hydrogenated-tallow ammonium montmorillonite. The nanocomposites are prepared via the direct melt intercalation technique using a conventional twin-screw extruder. Dynamic mechanical thermal analysis of the nanocomposites is conducted using two different test setups. The dynamic mechanical relaxation spectra show an increase in the storage modulus of the nanocomposite over the entire temperature range under study as compared to the pristine polymer (except in the transition region from 70 to 80 °C). These results are analyzed using the empirical Havriliak–Negami (HN) equation. The four temperature independent HN parameters (α, β, E_0, and E_∞) and one temperature dependent parameter (τ, the relaxation time) are determined by solving the HN equation for each temperature over the range of temperatures. The calculated moduli results fit well with the experimental values of the relaxation spectra for the nanocomposites. This study shows that the HN model can be applied to polymer layered silicate nanocomposites, and it can be used to predict their dynamic mechanical properties over a wide range of temperatures and frequencies *a priori*. © 2004 Wiley Periodicals, Inc. J Polym Sci Part B: Polym Phys 42: 2657–2666, 2004

Key words: nanocomposites; organoclay; viscoelastic properties; dynamic mechanical relaxation; Havriliak–Negami equation

INTRODUCTION

Research involving studies on inorganic and organic classes of hybrid materials has recently become an important area of investigation. Out of these materials, layered silicate based polymer nanocomposites have attracted considerable interest technologically and academically.[1–8] This is mainly due to the exceptional property enhancement these composites are able to achieve and the wide variety of applications in which polymer layered silicate (PLS) nanocomposites can be used.

Although many researchers have been successful in gaining insight into the science and technology of PLS nanocomposites, there is still much information to be covered before a complete understanding of how to prepare better nanocomposites is achieved. (A better understanding of nanocomposite properties is necessary for this.) However, it is not always possible to carry out every single experiment for optimizing product performance. Limiting the set of experiments and predicting the remaining set of data based on various empirical functions can typically overcome this limitation. This analysis has been

Correspondence to: J. P. Jog (E-mail: jyoti@che.ncl.res.in)
Journal of Polymer Science: Part B: Polymer Physics, Vol. 42, 2657–2666 (2004)

widely applied to predict polymer dynamic mechanical properties over a wide range of temperatures and frequencies. Because of their viscoelastic properties, polymers have been interesting objects for dynamic mechanical investigations for a long time.[9] It is now well known that PLS nanocomposites exhibit better mechanical properties compared to pristine polymers. In our recent articles we have reported the dynamic mechanical properties of PLS nanocomposites using a variety of polymer–clay combinations.[10–15] There are a number of models that describe the dynamic mechanical and dielectric relaxation behavior in polymers in the frequency and time domains. The most frequently used empirical equations for this purpose are the Havriliak–Negami (HN)[16,17] and Williams–Watts equations.[18,19]

The HN equation that relates the complex modulus (E^*) to the rubbery regime modulus at low frequencies (E_0) and the glassy regime modulus at high frequencies (E_∞) can be written as

$$E^*(\omega) = E_\infty + \frac{E_0 - E_\infty}{[1 + (i\omega\tau)^\alpha]^\beta} \quad (1)$$

where ω is the angular frequency ($\omega = 2\pi f$), τ is the relaxation time, i is the unit imaginary number ($i = \sqrt{-1}$), and α and β are the two adjustable fitting parameters. Here, α is related to the width of the loss peak and β controls the asymmetry of the loss peak. In this model α and β can both vary between $0 < \alpha \leq 1$ and $0 < \beta \leq 1$. In order to analyze the viscoelastic data using the HN model, it is necessary to incorporate the temperature dependence of the complex modulus [$E^*(T)$]. There are various methods of achieving this, including the one described by Alig et al.[20] In the present study we employ the strategy proposed by Szabo and Keough for fitting the HN model to the dynamic mechanical thermal analysis (DMTA) data pertaining to PLS nanocomposites.[21] In addition, the HN model is also fitted to the DMTA data of the pure polymer from which the nanocomposite has been derived. For fitting the HN model, single frequency DMTA data gathered over a range of temperatures are used; the model obtained thereby allows the prediction of the complex modulus over a wide range of temperatures and frequencies. The two-step procedure is described for estimating the time dependent and time independent parameters of the HN model as applied to the DMTA data of the pure polymer and nanocomposite. Using this analysis, we are able to predict the polymer nanocomposite dynamic mechanical properties over a wide range of temperatures and frequencies.

EXPERIMENTAL

Materials

The copolyester used in this study was poly(ethylene glycol-*co*-cyclohexane-1,4-dimethanol terephthalate) (PETG, grade EASTAR copolyester 6763) acquired from Eastman Chemical Company. PETG is an amorphous copolymer with a number-average molecular weight (M_n) of approximately 26,000 g mol^{-1}; it consists of cyclohexane dimethanol, ethylene glycol, and terephthalic acid in a molar ratio of approximately 1:2:3. The clay used in the study was kindly provided by Southern Clay Products, and it has the trade name Cloisite 25A (C25). The organically modified clay was prepared by the reaction of a tallow based compound containing quaternary ammonium counterions with montmorillonite clay. The organic compound used for this purpose was (2-ethyl-hexyl)dimethyl hydrogenated tallow. The reaction results in the exchange of sodium ions with ammonium ions. The quaternary ammonium intercalants contained a mixture of alkanes (~65% C18, ~30% C16, and ~5% C14). The cation exchange capacity of the C25 clay was 95 meq/100 g and the organic content was 34%, which was reported in the product literature. The clay was used as received with no additional purification steps.

Melt Processing

Premixed PETG and organoclay C25 were melt blended in a twin-screw extruder (Berstoff ZE-25) with corotating and intermeshing 25-mm screws (length/diameter = 41.5) at a barrel temperature profile of 170–210 °C and a screw speed of 100 rpm. The residence time inside the extruder was approximately 3.0 min under the processing conditions used in this work. The polymer and organoclay were dried in an air circulatory oven at a preset oven temperature of 70 °C for 27 h. One composition containing a 5:95 (w/w) ratio of organoclay to polymer was used in this study. The obtained strands were pelletized and dried at 70 °C for 24 h.

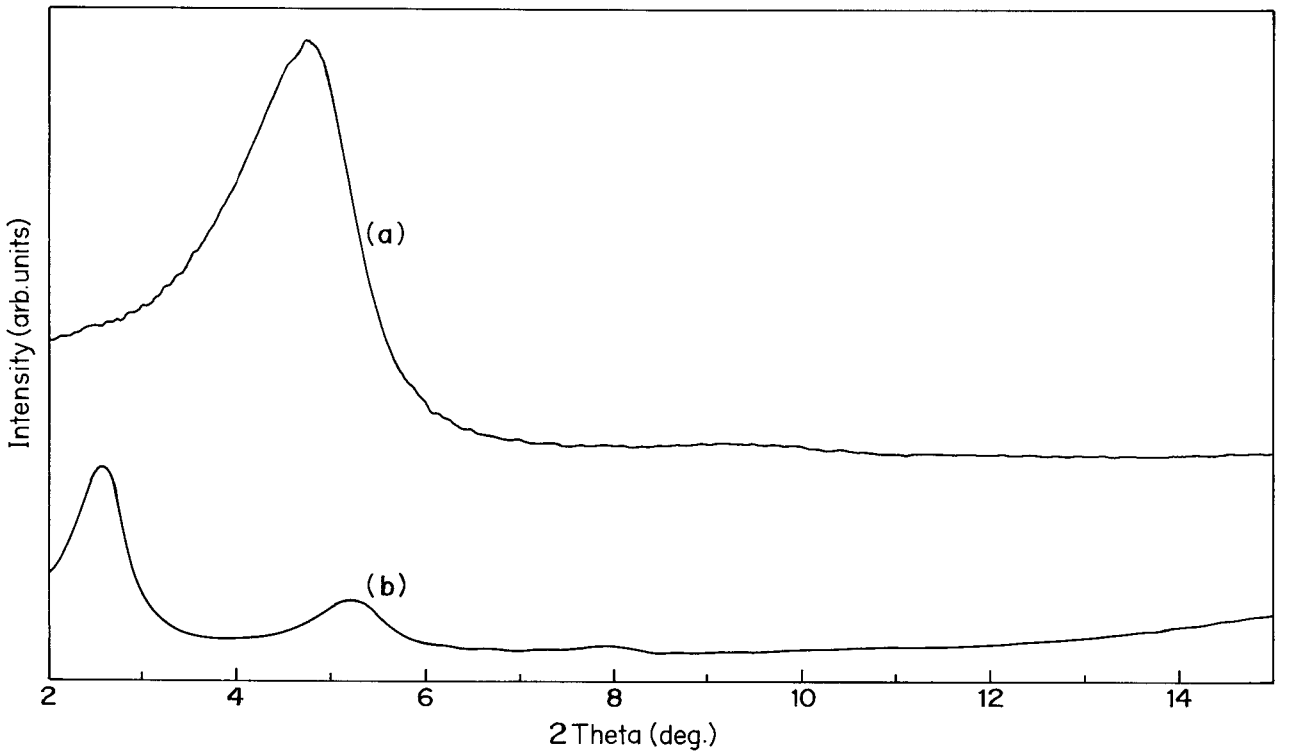

Figure 1. X-ray diffraction data for (a) organically modified layered silicate C25 and (b) polymer layered silicate nanocomposite PETGC25. The d_{001} of the nanocomposites has shifted to lower 2θ values, indicating intercalation of the polymer in the clay interlayer. The presence of d_{002} and d_{003} peaks in the nanocomposite suggests preservation of long-range order.

Methods of Characterization

The DMTA properties of the nanocomposites were studied using a Rheometrics Dynamic Mechanical Analyzer IIIE operating in rectangular tension/compression mode. The sample plates used in this study had 0.5-mm thickness and 10-mm width and were prepared by compression molding of the extruded pellets at 210 °C for 3 min using a Carver press (F-15181). The DMTA were performed in isothermal and nonisothermal conditions. The nonisothermal scans were performed over a temperature range of 35 to 90 °C at a heating rate of 5 °C min^{-1} at 0.05% strain and frequencies of 1, 10, and 100 rad s^{-1}. The isothermal frequency sweeps were carried out at two temperatures (35 and 70 °C) over the entire frequency range. The frequencies that were scanned ranged from 0.1 to 158.48 rads s^{-1}.

To ascertain the formation of the nanocomposite, microstructural evaluation of the samples was carried out using wide-angle X-ray diffraction (WAXD). The instrument used for this purpose was a Rigaku Dmax 2500 diffractometer with a copper target (λ = 1.54 Å, 40 kV, and 150 mA). An aluminum window was used as the sample holder on which the compression-molded samples with a uniform thickness of approximately 0.5 mm were mounted. All samples were scanned from 2θ = 2–15° at a scan rate of 4° min^{-1} at ambient temperature. The basal spacing of montmorillonite was estimated from the d_{001} peak in the X-ray diffraction pattern.

RESULTS AND DISCUSSION

Microstructure

The WAXD patterns of the organically modified layered silicate C25 and the nanocomposite PETGC25 are presented in Figure 1. The organically modified clay showed the d_{001} diffraction peak at a 2θ value of 4.7°, corresponding to a d-spacing of 1.8 nm. When these values are compared with those of the nanocomposite PETGC25,

it can be seen that the nanocomposite showed the d_{001} peak at a 2θ value of 2.6°, corresponding to a interlayer spacing of 3.3 nm. The nanocomposite also shows a d_{002} peak at $2\theta = 5.2°$, signifying a basal spacing of 1.6 nm and a small signal for d_{003} peak. The WAXD pattern of the nanocomposite suggests retention of higher orders. The increase in the d-spacing of the organically modified clay (i.e., $\Delta d = d_{NC} - d_{clay}$ is 1.5 nm) in the case of the nanocomposite indicates a high level of intercalation of the polymer in the clay gallery.

Optimization of Complex Modulus and Prediction of Dynamic Mechanical Properties

Figure 2 shows the temperature dependence of the storage modulus for the nonisothermal DMTA scans performed at 1, 10, and 100 rad s^{-1} over the temperature range of 35 to 90 °C. As is typical in cases of intercalated polymer clay nanocomposites, PETGC25 showed a higher dynamic modulus over that of PETG for the entire range of temperatures under study (except in the transition region from 70 to 80 °C), thus following a trend similar to our earlier viscoelastic studies on polymer clay nanocomposites.[10,11,14,15] The complex modulus is given in terms of its real part (storage modulus, E') and imaginary part (loss modulus, E''). The ratio of the loss modulus to the storage modulus, known as the "loss factor," is defined as

$$\tan \delta = \frac{E''}{E'} \tag{2}$$

It was established by Jones[22] that, for thermorheologically simple polymers, the corresponding Wicket plot, [log(tan δ)] versus log(storage modulus, E'), has an inverted U shape. Using various polymers, it was also demonstrated that all the loss factor complex modulus points determined using varying temperatures and frequencies lie on a unique curve. This observation, which is also valid for the E'' versus E' plots (known as Cole–Cole plots), was later confirmed for a number of other polymers by Szabo and Keough.[21] Using these observations as a basis, Szabo and Keough[21] recently proposed a simpler approach to perform DMTA in the context of the five-parameter HN model. Given complex modulus data covering a narrow frequency range or even a single frequency over a wide range of temperatures, the method of Szabo and Keough provides a means to estimate all five parameters of the HN model. This parameter estimation procedure makes two assumptions: the complex plane representation of the modulus is independent of the relaxation time τ, and τ is the only temperature dependent parameter in the HN model (i.e., α, β, E_0, and E_∞ are temperature independent). Because no specific functional dependence of τ on temperature is assumed, no additional parameter(s) than the five parameters appearing in the HN model (eq 1) need to be estimated. The above-described estimation procedure comprises step 1: plot the modulus in the complex plane and estimate α, β, E_0, and E_∞; and step 2: solve for τ at each temperature over which E^* measurements are conducted. We describe the detailed procedure for these two steps in the following sections.

Step 1: Estimation of α, β, E_0, and E_∞

Experimental E^* data at constant frequency (10 rad/s) and over varying temperatures were chosen for fitting the HN model. To begin, the relaxation time was set equal to 1 s and a set of trial values of α, β, E_0, and E_∞ was chosen such that for a specified frequency range the $E^*(\omega)$ values calculated from the HN equation lie in the same region as spanned by the experimental $E^*(T)$ values. The frequency region for such a match was found to be 10^{-5} to 10^{+10} Hz. For estimating α, β, E_0, and E_∞, Marquardt's multiparameter nonlinear function optimization algorithm[23] was used wherein the degree of fit between the model predicted complex modulus and the experimental modulus was evaluated in terms of two error functions, namely, the Cole–Cole (f_1) and Wicket (f_2) error functions.

In the Cole–Cole error function,

$$f_1 = \frac{\sum_{E'} |E''_{act} - E''_{cal}|^2}{\sum_{E'} |E''_{act}|^2} \tag{3}$$

where E'_{act} is the experimentally determined loss modulus and E'_{cal} is the calculated loss modulus.

In the Wicket error function,

$$f_2 = \frac{\sum_{E'} |\log(\tan \delta_{act}) - \log(\tan \delta_{cal})|^2}{\sum_{E'} |\log(\tan \delta_{act})|^2} \tag{4}$$

where $\tan \delta_{act}$ and $\tan \delta_{cal}$ are the experimentally determined and calculated loss factors, respectively.

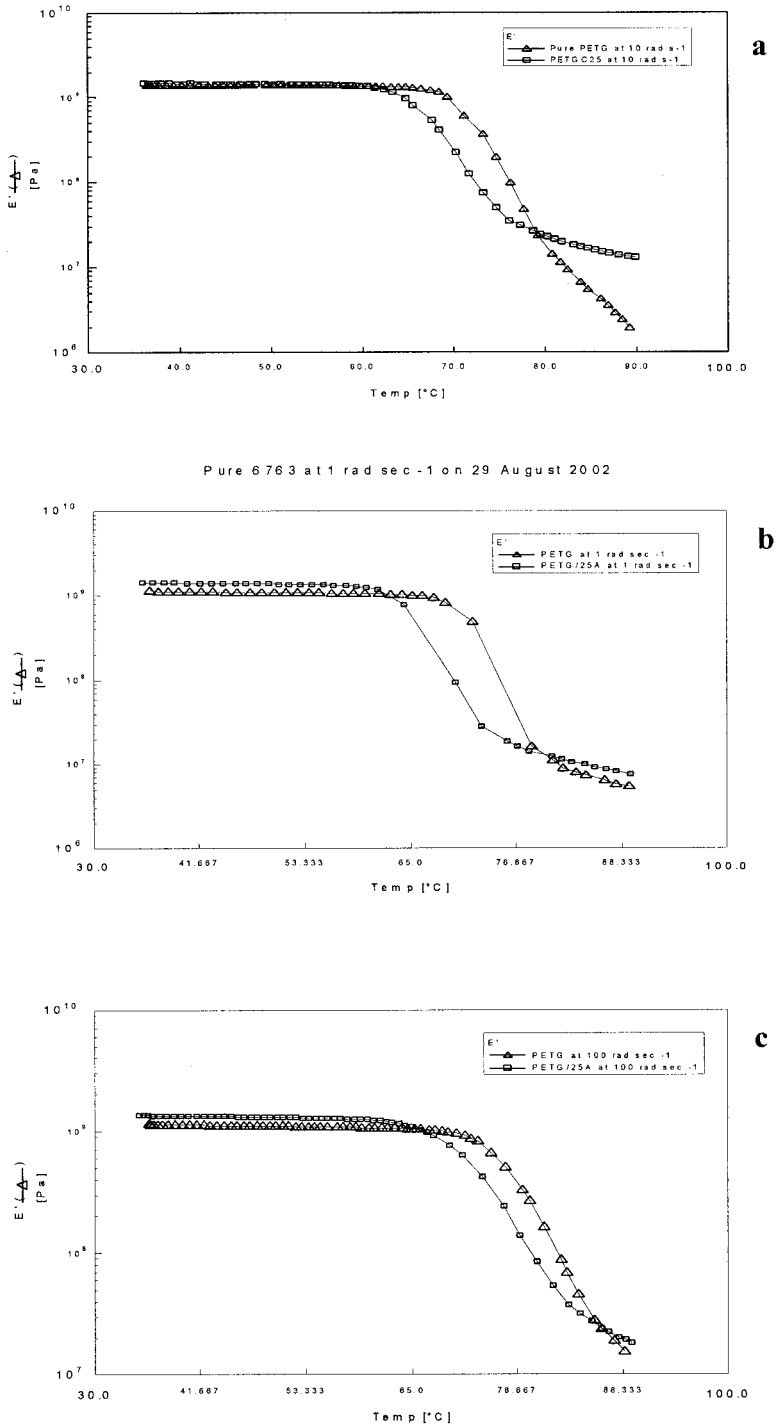

Figure 2. The temperature dependence of the storage modulus for pure PETG and PETGC25 for scans performed at (a) 10, (b) 1, and (c) 100 rad s^{-1}.

In order to achieve fast convergence to the optimal values of the four parameters, the Cole–Cole error function (f_1) was minimized first followed by minimization of the Wicket error function (f_2). The optimized values of α, β, E_0, and E_∞ obtained thereby for pure PETG and nanocomposite PETGC25 are listed in Table 1. Figure 3 depicts the Cole–Cole plots for the pure polymer and PETGC25. As can be noted, the optimal values of parameters α, β, E_0, and E_∞ provide a good

Table 1. Optimized Values of Temperature Independent HN Model Parameters

Material	α	β	E_0 (Pa)	E_∞ (Pa)
PETG	0.63	0.25	1.14×10^6	1.46×10^9
PETGC25	0.65	0.31	2.6×10^6	1.55×10^9

fit to the experimental modulus data pertaining to the pure polymer, as well as for the nanocomposite PETGC25. The shape of the relaxation process when viewed in a Cole–Cole plot is not dependent on the molecular weight of the polymer. However, it is governed by the nature and relative magnitudes of the intermolecular and intramolecular interactions. In turn, the shape of the relaxation process is dependent on a specific set of α and β parameters.[24,25] Thus, the numerical values of the α and β parameters will give an idea of the similarities and differences in the types of inter- and intramolecular interactions present in a polymer and PLS nanocomposite. The results shown in Table 1 indicate that the values of the α and β parameters in both pure PETG and PETGC25 are almost the same within experimental limitations. This suggests that the intermolecular and intramolecular interactions that arise in the polymer and PLS nanocomposite are almost identical.

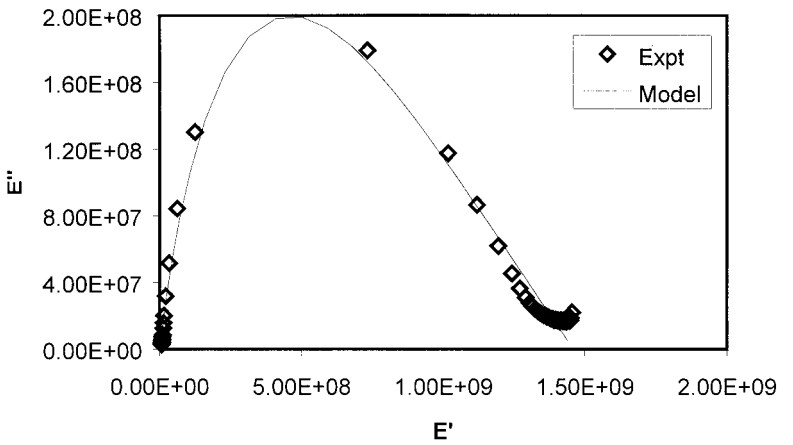

a

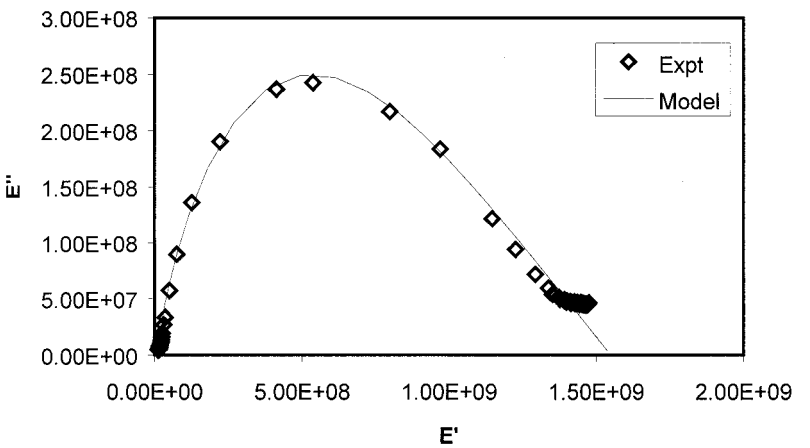

b

Figure 3. A Cole–Cole plot showing good fit of the Havriliak–Negami equation for (a) pure PETG and (b) nanocomposite PETGC25 at 10 rad s^{-1} (i.e., 1.59 Hz).

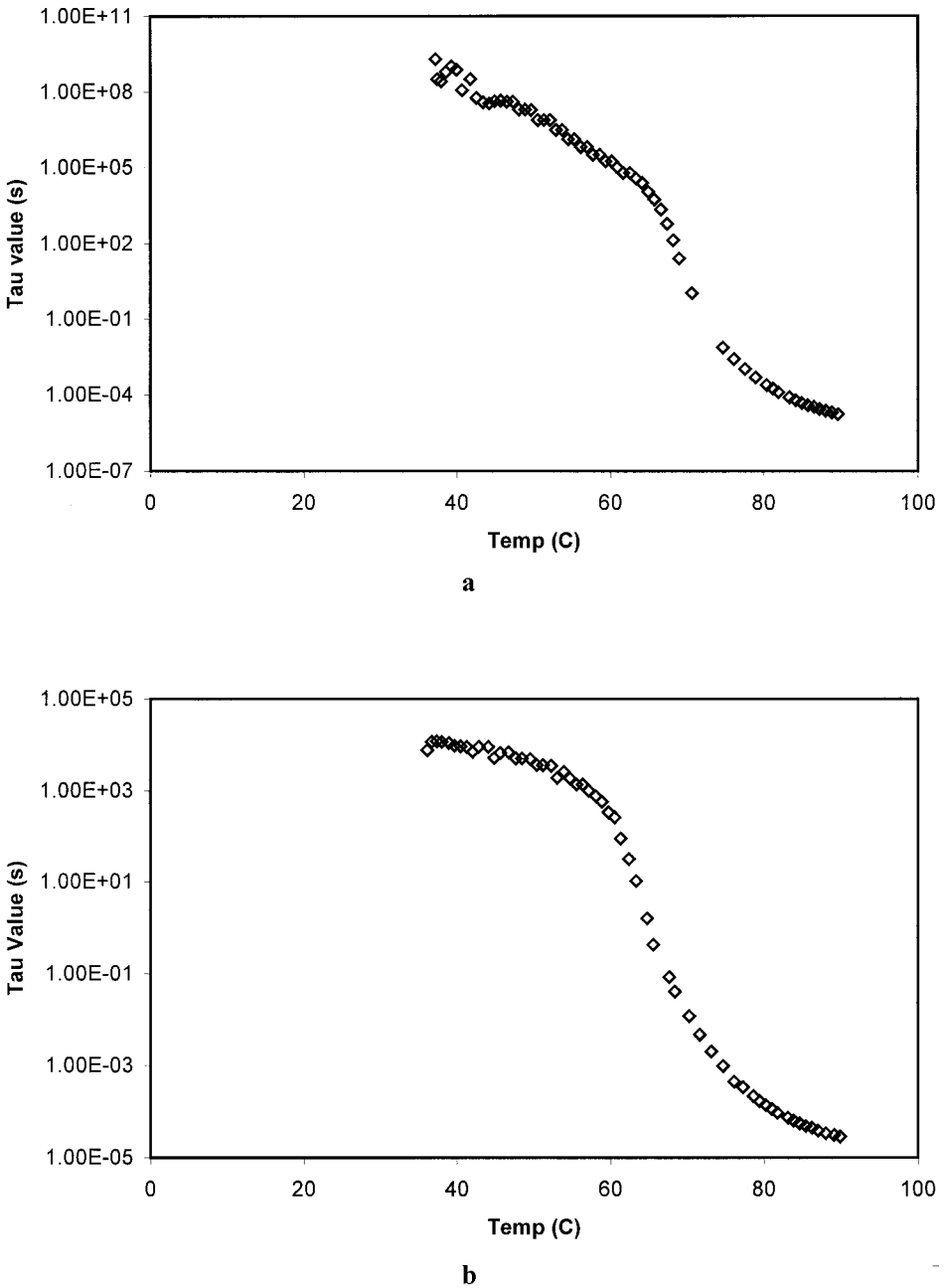

Figure 4. The relaxation time (τ) as calculated based on α, β, E_0, and E_∞ (Table 1) and the complex modulus (E^*) for (a) pure PETG and (b) nanocomposite PETGC25 .

Step 2: Estimation of τ

To compute the relaxation time (τ), the HN equation can be recast as given below.

$$\tau = \frac{1}{i\omega}\exp\left[\frac{1}{\alpha}\log\left\{\exp\left|\frac{1}{\beta}\log\left(\frac{E_0 - E_\infty}{E^* - E_\infty}\right)\right| - 1\right\}\right] \quad (5)$$

As can be seen, the right-hand side of this equation comprises experimentally measured values of E^* (which is a function of the frequency ω and temperature T) and the four temperature independent parameters α, β, E_0, and E_∞. Thus, the computation of τ is possible using the optimal values of the four parameters estimated in step 1 and the experimental values of the complex modulus $E^*(\omega, T)$. The τ values computed using the stated procedure are plotted in Figure 4, depicting the temperature dependence of the relaxation

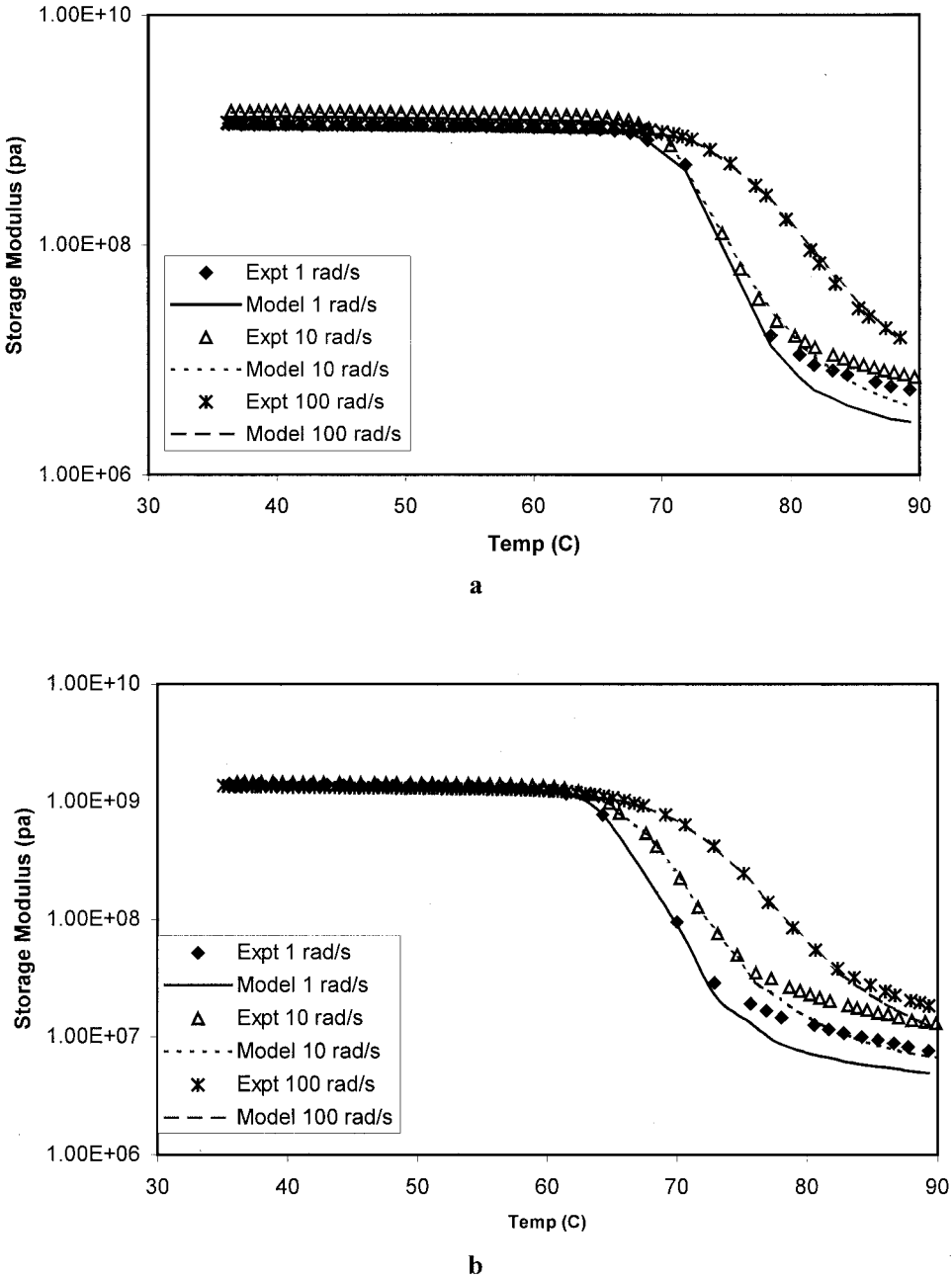

Figure 5. Experimental and calculated complex moduli over a range of temperatures for various frequencies for (a) pure PETG and (b) nanocomposite PETGC25.

time of the pure polymer and for the nanocomposite PETGC25. The figure shows that the relaxation time decreases with temperature, the rate of decrease being more pronounced in the glass-transition regions of the pristine polymer and the nanocomposite PETGC25.

Having estimated the four temperature independent parameters and the temperature dependent τ values (see Fig. 4) from single frequency DMTA data, the estimated values can be utilized in the HN equation to predict the complex modulus over a range of temperatures. For facilitating a comparison with the experimental DMTA data, the E^* predictions are restricted to the temperature range (35–90 °C) over which experimental E^* values are available. Figure 5 depicts a comparison of the experimental and HN model predicted storage modulus as a function of temperature for

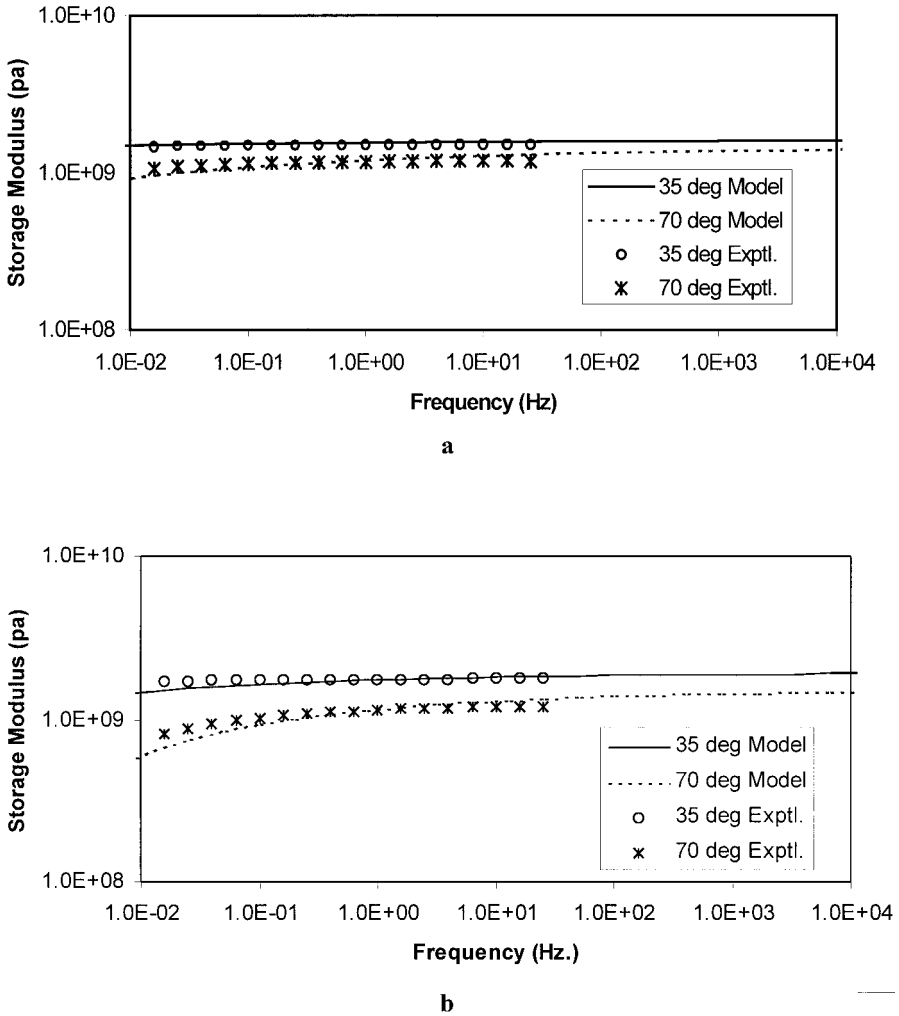

Figure 6. Experimental and calculated complex moduli over a wide range of frequencies at 35 °C (near room temperature) and 70 °C (at high temperature) for (a) pure PETG and (b) nanocomposite PETGC25.

pure PETG and nanocomposite PETGC25. From the plots in Figure 5 it is noted that for the three frequencies examined (1, 10, and 100 rad s^{-1}), the experimental and model predicted storage modulus values provide a very good match in the temperature range of 35–78 °C. In the temperature range from 78 to 90 °C, although the match is excellent for frequency equal to 100 rad/s, for the other two frequencies (1 and 10 rad s^{-1}) the model predicted E' values show minor deviations from their experimental values. The results indicate that the experimental data fit the HN relationship very well in most of the scan area. The high temperature predictions are less accurate than the low temperature predictions. This minor anomaly may be because the accuracy of the predicted properties is limited by the degree to which the experimental data may fit the HN relationship.

Parameters estimated in steps 1 and 2 can also be utilized in the HN equation for predicting the E^* value as a function of varying frequency at a constant temperature. Accordingly, the storage modulus values were computed over a wide frequency range (10^{-2}–10^{+4} Hz) at 35 (near room temperature) and 70 °C (a higher temperature but below the glass-transition temperature). Figure 6(a) presents the frequency dependence of the storage modulus of pure PETG at 35 and 70 °C. The corresponding HN fits are also plotted. The results indicate that the experimental data fit the HN equation very well for the storage modulus. The results shown in Figure 6(b) depict the storage modulus dependence on the frequency plots for the nanocomposite PETGC25.

These results indicate that the storage modulus data can be fitted very well to the HN function.

CONCLUSIONS

We investigated the solid-state viscoelastic behavior of intercalated nanocomposites based on PETG/clay using dynamic mechanical analysis. The nanocomposites showed an increased modulus over the entire temperature range studied. The X-ray analysis showed a shift in the d_{001} peak of the nanocomposites to a lower 2θ value as compared to the pristine polymer. These data showed that intercalated nanocomposites were obtained. A comparison of the experimental and HN model predicted storage moduli indicated that the experimental data fit the HN relationship very well in most of the scan area for both the temperature ramp and frequency sweep experiments. The most important outcome of this study is the successful employment of the HN relationship to predict the dynamic mechanical properties of polymer/clay nanocomposites over a wide range of temperatures and frequencies.

The Council of Scientific and Industrial Research, India, is gratefully acknowledged for awarding Senior Research Fellowships and research grants to the second and third authors (R.A.K. and S.N.). The authors thank Southern Clay Products for their generous gifts.

REFERENCES AND NOTES

1. Okada, A.; Fukushima, Y.; Kawasumi, M.; Inagaki, S.; Usuki, A.; Sugiyami, S.; Kurauchi, T.; Kamigaito, O. (Toyota Motor Co.) U.S. Patent 4,739,007, 1988.
2. Kawasumi, M.; Kohzaki, M.; Kojima, Y.; Okada, A.; Kamigaito, O. (Toyota Motor Co.) U.S. Patent 4,810,734, 1989.
3. Krishnamoorti, R.; Vaia, R. A.; Giannelis, E. P. Chem Mater 1996, 8, 1788.
4. Krishnamoorti, R.; Giannelis, E. P. Macromolecules 1997, 30, 4097.
5. Vaia, R. A.; Giannelis, E. P. Macromolecules 1997, 30, 7990.
6. Vaia, R. A.; Giannelis, E. P. Macromolecules 1997, 30, 8000.
7. Balazs, A. C.; Singh, C.; Zhulina, E. Macromolecules 1998, 31, 8370.
8. Galgali, G.; Ramesh, C.; Lele, A. Macromolecules 2001, 34, 852.
9. Ferry, J. D. Viscoelastic Properties of Polymers, 3rd ed.; Wiley: New York, 1980.
10. Kodgire, P.; Kalgaonkar, R.; Hambir, S.; Bulakh, N.; Jog, J. P. J Appl Polym Sci 2001, 81, 1786.
11. Hambir, S.; Bulakh, N.; Kodgire, P.; Kalgaonkar, R.; Jog, J. P. J Polym Sci Part B: Polym Phys 2001, 39, 446.
12. Priya, L.; Jog, J. P. J Polym Sci Part B: Polym Phys 2002, 40, 1682.
13. Wanjale, S. D.; Jog, J. P. J Polym Sci Part B: Polym Phys 2003, 41, 1014.
14. Kalgaonkar, R. A.; Jog, J. P. J Macromol Sci Part B: Phys 2004, B43, 417.
15. Kalgaonkar, R. A.; Jog, J. P. J Polym Sci Part B: Polym Phys 2003, 41, 3102.
16. Havriliak, S.; Negami, S. J Polym Sci Part C: Polym Symp 1966, 14, 99.
17. Havriliak, S.; Negami, S. Polymer 1967, 8, 161.
18. Williams, G.; Watts, D. C. Trans Faraday Soc 1970, 66, 80.
19. Williams, G.; Watts, D. C.; Dev, S. B.; North, A. M. Trans Faraday Soc 1971, 67, 1323.
20. Alig, I.; Tadjbakhsch, S.; Zosel, A. J. Polym Sci Part B: Polym Phys 1998, 36, 1703.
21. Szabo, J. P.; Keough, I. A. Thermochim Acta 2002, 392–393, 1.
22. Jones, D. I. G. J. Sound Vib 1990, 140, 84.
23. Marquadt, D. M. J Soc Ind Appl Math 1963, 11, 471.
24. Mansfield, M. L. J Polym Sci Polym Phys Ed 1983, 21, 787.
25. Havriliak, S., Jr. J Phys Chem 1990, 94, 4705.